Russian Journal of Earth Sciences

Evaluation of Displacements Caused by Strike-Slip Deformations Using Correlation Characteristics Based on Potential Field Data

N. P. Senchina*[,1], A. E. Asoskov[2], and G. D. Gorelik[1]

[1]St. Petersburg Mining University, St. Petersburg, Russia
[2]A. P. Karpinsky Russian Geological Research Institute, St. Petersburg, Russia
* **Correspondence to:** N. P. Senchina, n_senchina@inbox.ru

Abstract: The identification of faults is a common objective in geophysical potential field methods. Vertical discontinuities such as reverse faults, also known as tectonic faults, can easily be distinguished through their effect on gravity and magnetic fields, appearing as gradient zones or areas of change in the field. However, identifying strike-slip faults is one of the biggest challenges for potential field methods as they are characterized by a complex series of anomalies with varying signs in the fault zone, as well as displacement of anomaly axes between the strike-slipped blocks. The goal of this study is to suggest a transformation that would aid in the identification of shear zones through the calculation of the displacement along the discontinuity. The proposed approach involves calculating the correlation coefficient between parallel profiles using moving windows. The position of the window with the highest calculated correlation coefficient allows estimating of the discontinuity displacement magnitude. The method was tested using a synthetic field and data from the magnetic field of the Kolbeinsi Ridge.

Keywords: strike-slip, correlation, gravity exploration, magnetic exploration, interpretation

Citation: Senchina, N. P., Asoskov A. E., Gorelik G. D. (2023), Evaluation of Displacements Caused by Strike-Slip Deformations Using Correlation Characteristics Based on Potential Field Data, *Russian Journal of Earth Sciences*, 23, ES4013, EDN: NWCRGX, https://doi.org/10.2205/2023es000847

Introduction

The detection of fault displacements is a standard task for geophysical potential field methods interpretation. Drops, spills – fault displacements with vertical displacement – are well distinguished by gravity and magnetic fields as gradient zones or zones of field character change. Traces for detecting such zones can be well traced both manually and automatically – actually by fields or their transformations [*Asoskov and Senchina*, 2022; *Nikitin and Petrov*, 2007; *Saitgaleev et al.*, 2021]. The detection of strike-slip displacements is one of the most difficult tasks for potential field methods, as displacements are expressed as a complex chain of non-uniform anomalies in the zone of the fault itself, and by the displacement of anomaly axes between shifted blocks [*Asoskov*, 2022; *Tran et al.*, 2021]. The task of this work is to propose such a transformation that could help to detect displacement zones with the calculation of displacement along the fault. In this work, the object of study is only one feature of displacement – displacement itself, without taking into account the formation of anomalies by the structures of displacement themselves – pull-apart basins, folds, pop-up ridges and so on.

The relevance of shear structures studying is great. Shear faults are interesting in prospecting and exploration of hydrocarbon deposits [*Gusev et al.*, 2020; *Prishchepa et al.*, 2021], as they can form pull-apart basins (troughs) with heavy sedimentation [*Egorov et al.*, 2022; *Koronovsky et al.*, 2009; *Sohrabi et al.*, 2019]. Tectonic-magmatic and disjunctive factors associated with faults, including strike-slip nature, affect the localization of ore-bearing structures [*Alekseev*, 2020, 2021]. The structure of ore bodies is often controlled by

Research Article

Received: 20 February 2023
Accepted: 10 April 2023
Published: 7 December 2023

shears [*Arkadiev*, 1969; *Movchan et al.*, 2022], since emerging spalls and cracks form a void space for ore deposition in a well-permeable zone [*Il'chenko et al.*, 2022; *Yakovleva et al.*, 2022]. Tectonic disturbances of shear nature form wide zones of increased rock fracturing, which can be significant in assessing the quality of facing stone [*Isakova et al.*, 2021], in studying the stability of structures or mine workings [*Kazanin et al.*, 2021]. In addition, shifts are of interest from the standpoint of general geology, when specifying the structure and evolution of territories [*Ageev et al.*, 2019].

Description of Calculation Methodology

The proposed approach involves calculating the correlation coefficient between moving windows of parallel profiles. In this case, the position of the window with the maximum calculated correlation coefficient can be identified, and this position will characterize the magnitude of the offset along the fault. The correlation coefficient, a parameter that characterizes the degree of linear relationship between two samples [*Wherry*, 1984], varies from −1 to 1. The linear correlation coefficient is defined as

$$k = \frac{\sum((x_i - \overline{x}) \cdot (y_i - \overline{y}))}{\sqrt{\sum (x_i - \overline{x})^2 \cdot \sum (y_i - \overline{y})^2}},$$

where x_i – values taken in the sample X, y_i – values taken in the sample Y; $\overline{x}$ – average in X, $\overline{y}$ – average in sample Y.

The order of calculations for the initial data presented in the form of a matrix of field values (areal distribution) is assumed in a simplified version as follows:

1. choice of elongated sliding windows direction (along the supposed strike-slip faults), or sequential enumeration of directions;
2. selection of the window size in accordance with the most pronounced spatial frequencies of the analyzed signal;
3. choice of distance between moving windows;
4. performing shifts of the second window at a fixed position of the first with the calculation of the correlation coefficient for each shift;
5. analysis of obtained correlation coefficients with the selection of a maximum;
6. determination of the shift at which the maximum correlation coefficient is achieved;
7. assignment to the cell of the first resulting matrix located between the sliding windows, the value of the obtained maximum of the correlation coefficient;
8. assigning to the cell of the second resulting matrix, located between the sliding windows, the value of the resulting offset, this is the main desired result, corresponding to the magnitude of the strike-slip fault.

To explain the calculations, consider a field model consisting of 6 survey points with 6 profiles each, making a total of 36 cells. Sample X is a window, for example, 3 cells in size within the second column, while sample Y moves in the fourth column. The index corresponding to the shear during this movement is called s. For each position of window Y, we calculate the correlation coefficient k, and on the graph we highlight the position of the maximum. The value of the maximum obtained is recorded for the calculation point as the variable $k_{\max}$, and the corresponding strike-slip is recorded as $s_{\text{strike-slip}}$. As shown in the example, the highest correlation, equal to 1, is achieved when the Y window is strike-slipped relative to the X window by one unit, as reflected in the graph (Figure 1). The strike-slip magnitude is identified by the value $s_{\text{strike-slip}}$ at which the maximum correlation coefficient is reached.

If we build a map of the main calculation result – the magnitude of the strike-slip – a zone in the center of the calculation area along the synthesized strike-slip zone will be highlighted with values of +1 ("+" corresponds to right-lateral strike-slip), while for the rest of the area – 0 (no strike-slip). The resulting map is smaller, since there is no way to calculate the coefficient for side points (Figure 2).

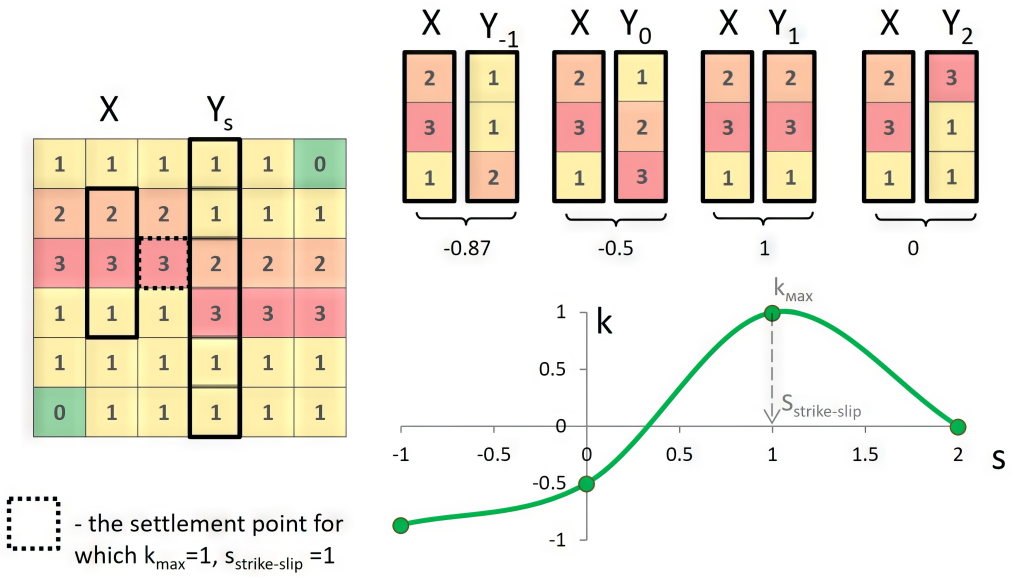

Figure 1. Calculation of correlation coefficient at different strike-slips of the *Y* window.

For this most simplified case, the strike-slip is correctly identified, and it is worthwhile to test the algorithm on more complex models. Below there are the test results for one of the simplest field variants, in which there are two anomalies complicated by a strike-slip.

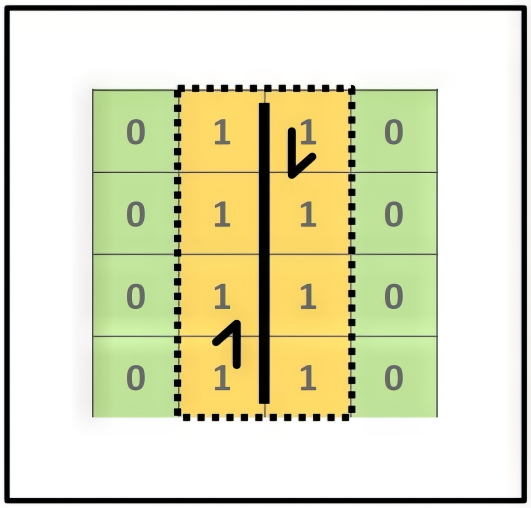

Figure 2. Result of the calculation of the strike-slip value for the original data shown in Figure 1 and position of the strike-slip line.

The Testing of the Algorithm

Consider a field that features synthesized linear anomalies of latitudinal stretching with a strike-slip in the *x*-coordinate area, equal to 13.5 km (Figure 3). The anomalies are positive and negative and do not change along the axis of the anomalies. The shift, simulating a strike-slip, has a meridional stretching – so this model is the simple for interpretation. The strike-slip is implemented in a northern direction (left-side strike-slip) by magnitude 8 km. A low-amplitude random noise is added to the field. The signal-to-noise ratio is approximately 100. It is assumed that the results are equally applicable to both gravity and magnetic field data, so in the task, we will consider a hypothetical potential field in conventional units.

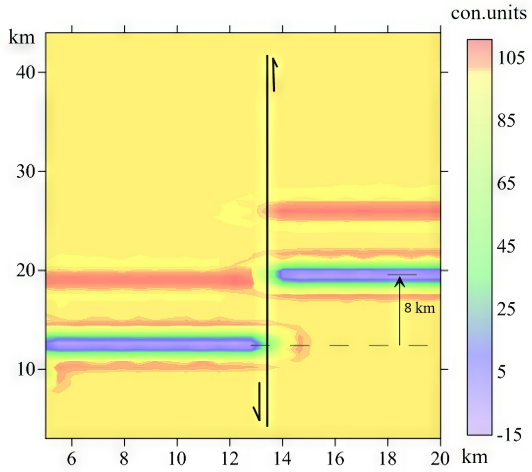

Figure 3. Synthetic field for testing the strike-slip identification algorithm.

For comparison of the results of the proposed algorithm with existing solutions, we will perform the calculation of some transformations typically used for solving geotectonic problems to show that when strike-slip zones are highlighted, they are ineffective. Thus, it is considered advisable to calculate transformations such as "tilt derivative" (TDR), "total horizontal gradient", as well as an option for automatic tracing of anomaly axes (using the "Reana" macros (author M. B. Shtokalenko) [*Shtokalenko*, 2018]. Examples of transformation calculation results are presented below. It can be seen that none of them give any anomaly along the strike-slip zone. In general, this result is almost obvious, as the transformations usually highlight any anomalies, but separate anomalies along the strike-slip zone are not introduced here, only the strike-slip is specified (Figure 4).

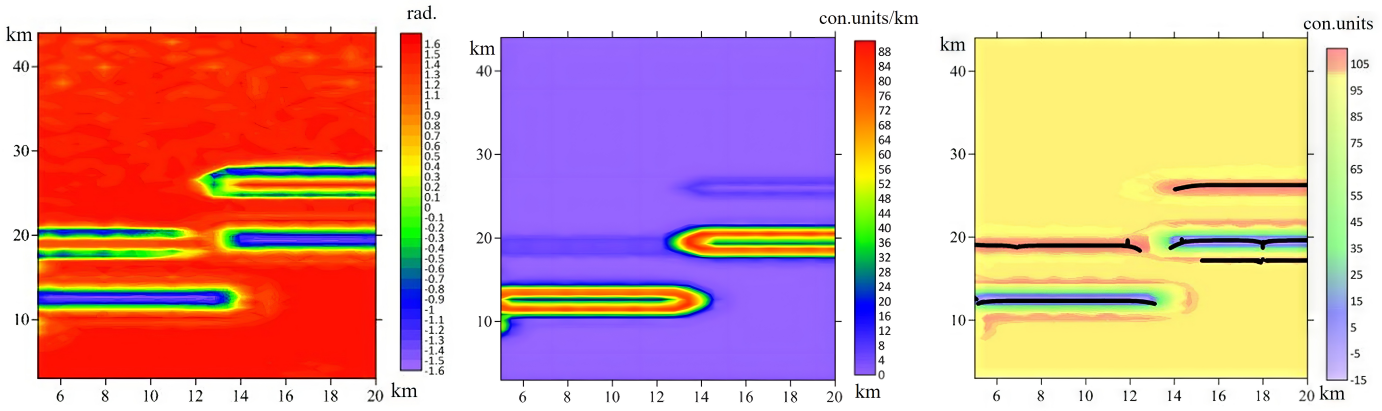

(a) "Tilt derivative" (TDR) **(b)** "Total horizontal gradient" **(c)** Anomaly axis lines ("Reana")

Figure 4. Some traditional transformations of the field shown in Figure 3.

Let's perform the calculation according to the proposed methodology. The result is described by two parameters – the maximum paired correlation coefficient for the sliding window, and the magnitude of the strike-slip at which this maximum is reached. The algorithm is currently developed poor enough, these are the first tests of the methodology, so we take samples (profiles with moving windows) as shown in Figure 1 – along the longitudinal direction. In general, in the future, it is necessary to move on to trying different directions, as well as testing the algorithm when changing the window length, the step between compared profiles, etc. However, as the first results of testing, we present the following. As shown on the correlation coefficient map – Figure 5a – (values less than 0.25 are not of interest to us), the maximum correlation – about 1 – is achieved on parts of

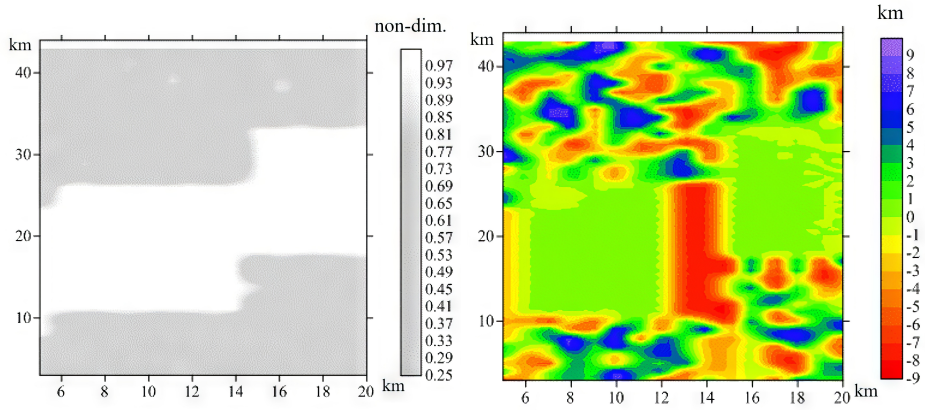

Figure 5. Calculation result of the value of the paired linear correlation coefficient (a) and strike-slip magnitude (b) for the original data shown in Figure 3.

the map where linear anomalies are significant and random noise is of low significance. Such parts of the map are colorless, while low-value coefficient parts are filled with gray color.

The offset (Figure 5b) is defined in the range from −9 to 9 km, one pronounced anomaly runs along the strike-slip that needed to be extracted, and there is also a chaotic picture in the part where the correlation coefficient is relatively low. Since the chaotic distribution of offsets is an expression of interference that has no relationship to the strike-slip, these parts of the offset map can be screened using the correlation coefficient map, partially transparent. Then, the bright parts with a well-traceable anomaly will be visible, and one bright strike-slip in the 13.5 pickup area will be highlighted. Positive values of offsets correspond to a right strike-slip, negative values correspond to a left strike-slip. It can be stated that the result is exactly defined as left-handed with an offset of about 8 km (Figure 6).

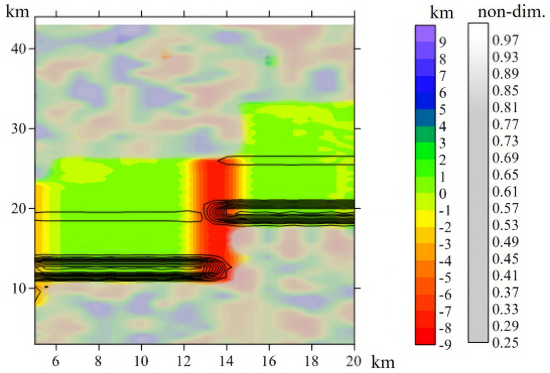

Figure 6. A summary result scheme (black contours correspond to the original field) for the original data shown in Figure 3.

This example presents a methodology for calculating and an example of the result in the most simplified conditions. It is shown that the algorithm correctly identifies the strike-slip zone and it makes sense to improve the algorithm for work in more complex conditions.

Practical Example

For the first practical test of the algorithm, the Kolbeinsey Ridge and its surroundings were selected. The ridge is a segment of the Mid-Atlantic Ridge located to north of Iceland

in the Arctic Ocean. In Iceland, transform faults are exposed on the surface, for example, the Reykjanes fault. Similar structures complicate the Mid-Oceanic ridges everywhere and are the most simple in configuration manifestation of strike-slip [*Hensen et al.*, 2019] – without the formation of pronounced structures such as "horse tail", fault duplexes, pull-apart basins, flower-like, palm-tree-like structures, etc., typical for strike-slips in areas with a powerful heterogeneous crust and sedimentary cover [*Frolova et al.*, 2019; *Karimova and Bornyakov*, 2021]. As mathematical and physical modeling shows, the character of morphostructural segmentation of spreading axes depends mainly on the degree of mantle heating and lithosphere thickness, the spreading slope and declination, and the existence of structural inhomogeneities with increased lithosphere strength [*Dubinin and Grokholsky*, 2020; *Mansurova*, 2010], and is reflected mainly in the magnitude of displacement, the contribution of the rotational component, and the "frequency" of the location of transform zones. In the magnetic field of the research platform, the breakaway with a strike-slip character of the field is clearly visible, which is also related to the choice of the section [*Gaina et al.*, 2011; *Kashubin et al.*, 2021; *Petrov and Poubelier*, 2019]. The displacements are associated with transform faults located subperpendicular to the divergent deep faults, which are formed during spreading [*Akhverdiev et al.*, 2018]. Transform faults form systems of parallel strike-slips located within active extension structures. Within the polygon, several such strike-slip zones can be distinguished [*Brandsdóttir et al.*, 2015], transform faults are identified here based on bathymetry data and confirmed by the results of geophysical investigations [*Chunguan et al.*, 2019].

To set a simple task for the algorithm at the current stage of work, let's select a small area of the map and rotate it. Calculate the correlation coefficient in a sliding window and the shift value according to the algorithm described above, with a window length corresponding to 50 km and the assumed vertical (when looking at the map) orientation of the strike-slip. The shifts due to at least two distinct offsets that are clearly visible on the magnetic field map (Figure 7) are quite obvious and are approximately 20 km.

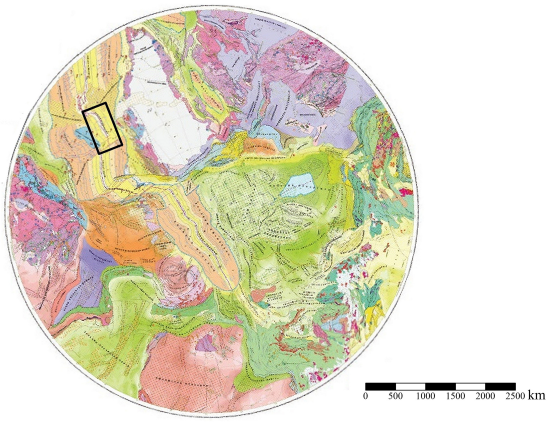

(a) [*Jackson et al.*, 1998; *Petrov and Poubelier*, 2019] map of anomalous magnetic field

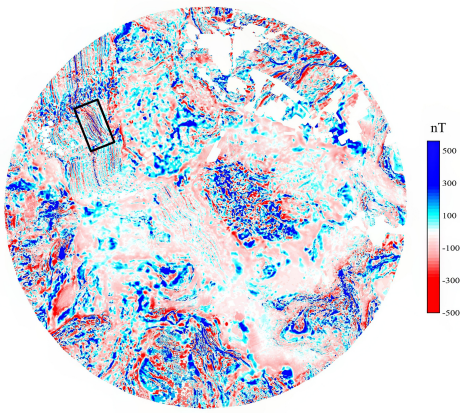

(b) [*Gaina et al.*, 2011] with study area; fragment of the geological map

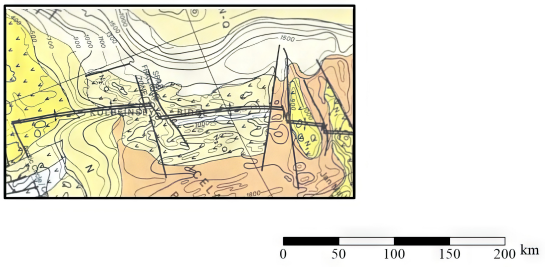

(c) and magnetic anomalies map

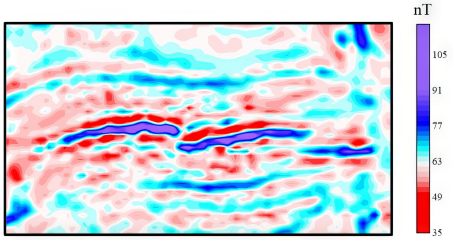

(d) for the algorithm testing

Figure 7. Test site for the algorithm's practical testing – the vicinity of the Kolbeinsi ridge, a small-scale geological map.

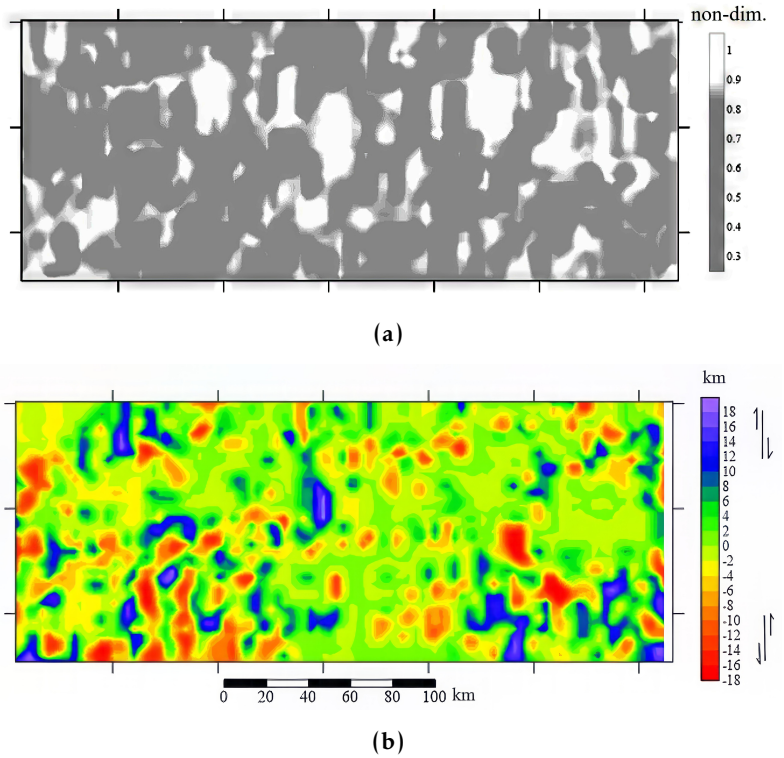

Figure 8. Result of calculating the paired linear correlation coefficient (a) strike-slip magnitude (b) for the data shown in Figure 7.

As a result, a displacement map was obtained, showing only one of the displacements visible in Figure 7. The magnitude of the displacement was determined fairly well, as 18 km, with a right-lateral strike-slip. Several other small similar structures have also been identified, mostly also corresponding to rightward shifts (Figure 8). It should be noted that the resulting maps are smaller than the original, as it is not possible to calculate the required characteristics for the edge parts. We will transfer the displacement axes from Figure 9 to the anomalous magnetic field map (Figure 10). For the relatively large strike-slip marked with the number 1, we will show its direction. Unfortunately, the strike-slip marked with the number 2 in the results of the algorithm was not highlighted as expected. The probable reason is its more complex manifestation in the magnetic field – the displacement axis is not perpendicular to the anomaly axes (ridge), but goes at an angle near 45 °C, which for the algorithm at its current stage of development is not accessible. It seems that an anomaly has been noticed below the expected position of the second strike-slip and it has a different sign. This means that the strike-slip here has a seemingly

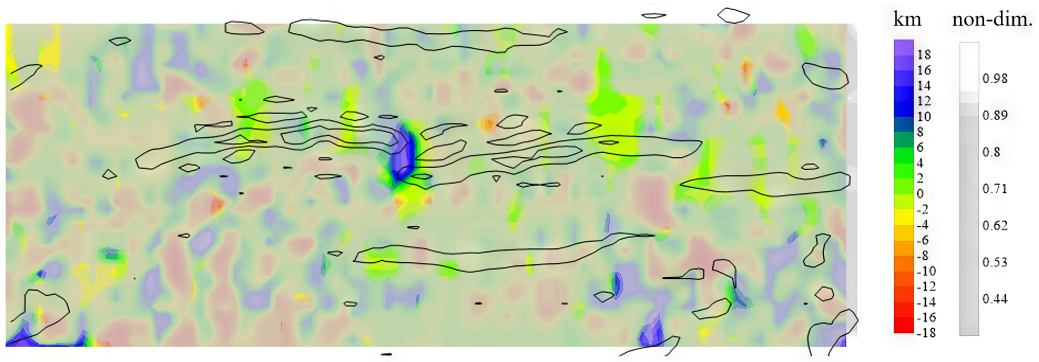

Figure 9. Summary result diagram. The black contours correspond to the original field, the colors correspond to the magnitude of the strike-slip, the gray mask is overlayed on the areas where the correlation coefficient is relatively low.

opposite orientation. This is probably due to the current features of the algorithm, which have correlated the crest axis with one of the anomalies located on the map below. This "false" strike-slip is defined as left-sided, not a continuation of the right-sided shift of the main structure. This result is masked by the map of the maximum correlation coefficient. It seems that it is less than 0.89 in this area, so this area cannot be determined as the final result of the algorithm. However, it is important to pay attention to potentially arising problems of this nature for further improvement of the algorithm.

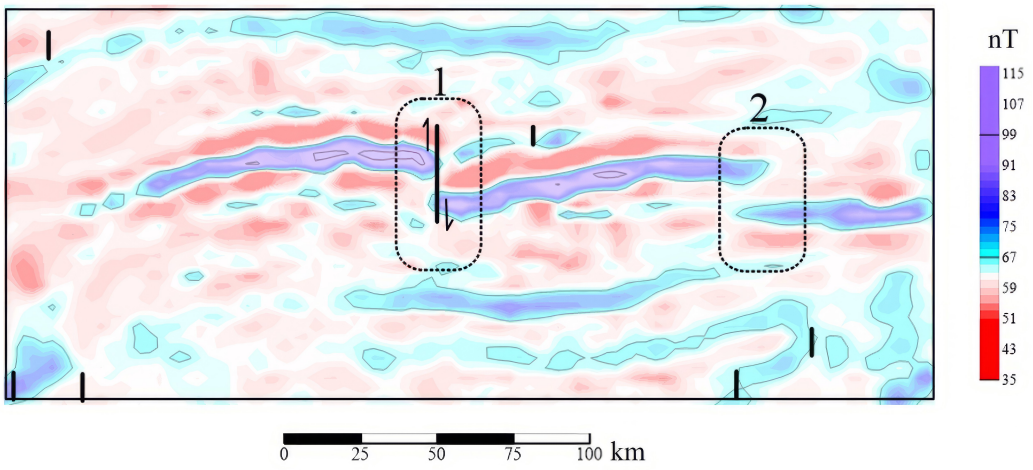

Figure 10. Map of the result of the magnetic field anomaly interpretation. Number 1 indicates a confidently identified strike-slip by the algorithm, number 2 is a missed one. Black vertical segments correspond to possible strike-slips with a small offset, which were uncertainly identified by the algorithm.

The methodology of strike-slips lateral displacement estimation is briefly described in the work, and the feasibility of the algorithm is shown on a simple example and on real data.

The greatest difficulties in further development of the algorithm are probably the possibility of strike-slips in different directions, when the directions of extension of the main anomalies are orthogonal (in the current examples). It is also likely that the detection of real strike-slips will be complicated due to the formation of derivatives from the strike-slips of structures, such as ridges, basins, and systems of fault ruptures. Nevertheless, the work appears to be promising and of practical significance.

Acknowledgments. The authors have no funding to report.

References

Ageev, A. S., R. K. Ilalova, A. M. Duryagina, and I. V. Talovina (2019), A link between spatial distribution of the active tectonic dislocation and groundwater water resources in the Baikal-Stanovaya shear zone, *Mining Informational and analytical bulletin*, *5*, 173–180, https://doi.org/10.25018/0236-1493-2019-05-0-173-180 (in Russian).

Akhverdiev, A. T., N. T. Karimova, D. A. Kozhevnikova, and T. E. Karimova (2018), Origin of deep faults and their classification, *Science, Technology and Education*, *8*(49), 15–22 (in Russian).

Alekseev, V. (2020), Deep structure and geodynamic conditions of granitoid magmatism in the Eastern Russia, *Journal of Mining Institute*, *243*, 259, https://doi.org/10.31897/pmi.2020.3.259.

Alekseev, V. (2021), Tectonic and magmatic factors of Li-F granites localization of the East of Russia, *Journal of Mining Institute*, *248*, 173–179, https://doi.org/10.31897/pmi.2021.2.1.

Arkadiev, N. A. (1969), On the structures of ore fields in connection with shear deformations, *Journal of Mining Institute*, *58*(2), 100–105 (in Russian).

Asoskov, A. E. (2022), Modeling the formation of geophysical anomalies disturbed by shear deformations, in *Fundamental and applied scientific research: topical issues, achievements and innovations*, pp. 32–34, International Scientific and Practical Conference, Sterlitamak (in Russian).

Asoskov, A. E., and N. P. Senchina (2022), Interpretation of geophysical data in the presence of shear deformations (on the example of a synthetic model), *Interactive science*, (10 (75)), 8–11, https://doi.org/10.21661/r-557897 (in Russian).

Brandsdóttir, B., E. E. E. Hooft, R. Mjelde, and Y. Murai (2015), Origin and evolution of the Kolbeinsey Ridge and Iceland Plateau, N-Atlantic, *Geochemistry, Geophysics, Geosystems*, *16*(3), 612–634, https://doi.org/10.1002/2014gc005540.

Chunguan, Z., L. Xiang, Y. Bingqiang, and S. Lijun (2019), Quality Evaluation of Offshore Data in the Earth Magnetic Anomaly Grid (2-arc-Minute Resolution): Taking the Southern Section of the Kolbeinsey Ridge in the Arctic Region as an Example, *Advances in Earth Science*, *34*(3), 288–294, https://doi.org/10.11867/j.issn.1001-8166.2019.03.0288.

Dubinin, E. P., and A. L. Grokholsky (2020), Specific features of structure formation during the development of the lithosphere of the Gulf of Aden (physical modeling), *Geodynamics & Tectonophysics*, *11*(3), 522–547, https://doi.org/10.5800/gt-2020-11-3-0489.

Egorov, A., N. Bolshakova, D. Kalinin, and A. Ageev (2022), Deep structure, tectonics and geodynamics of the Sea of Okhotsk region and structures of its folded frame, *Journal of Mining Institute*, *257*, 703–719, https://doi.org/10.31897/pmi.2022.63.

Frolova, N. S., T. V. Kara, and A. F. Chitalin (2019), Physical modeling of shear zones of varying complexity to identify areas of increased fluid permeability, *Dynamic geology. Electronic scientific and educational journal*, *1*, 29–47 (in Russian).

Gaina, C., S. C. Werner, R. Saltus, and S. Maus (2011), Chapter 3 Circum-Arctic mapping project: new magnetic and gravity anomaly maps of the Arctic, *Geological Society, London, Memoirs*, *35*(1), 39–48, https://doi.org/10.1144/m35.3.

Gusev, E., A. Krylov, D. Urvantsev, Y. Goremykin, and P. Krynitsky (2020), Geological structure of the northern part of the Kara Shelf near the Severnaya Zemlya archipelago according to recent studies, *Journal of Mining Institute*, *245*, 505–512, https://doi.org/10.31897/pmi.2020.5.1.

Hensen, C., J. C. Duarte, P. Vannucchi, A. Mazzini, M. A. Lever, P. Terrinha, L. Géli, P. Henry, H. Villinger, J. Morgan, M. Schmidt, M.-A. Gutscher, R. Bartolome, Y. Tomonaga, A. Polonia, E. Gràcia, U. Tinivella, M. Lupi, M. N. Çağatay, M. Elvert, D. Sakellariou, L. Matias, R. Kipfer, A. P. Karageorgis, L. Ruffine, V. Liebetrau, C. Pierre, C. Schmidt, L. Batista, L. Gasperini, E. Burwicz, M. Neres, and M. Nuzzo (2019), Marine Transform Faults and Fracture Zones: A Joint Perspective Integrating Seismicity, Fluid Flow and Life, *Frontiers in Earth Science*, *7*, https://doi.org/10.3389/feart.2019.00039.

Il'chenko, V., E. Afanasieva, T. Kaulina, L. Lyalina, E. Nitkina, and O. Mokrushina (2022), Litsa uranium ore occurrence (Arctic zone of the Fennoscandian Shield): new results of petrophysical and geochemical studies, *Journal of Mining Institute*, *255*, 393–404, https://doi.org/10.31897/pmi.2022.44.

Isakova, E. P., S. M. Daniliev, and T. A. Mingaleva (2021), GPR for mapping fractures for the extraction of facing granite from a quarry: A case study from Republic of Karelia, *E3S Web of Conferences*, *266*, 07,007, https://doi.org/10.1051/e3sconf/202126607007.

Jackson, H. R., B. G. Lopatin, and A. V. Okulich (Eds.) (1998), *Geological map: Circumpolar geological map of the Arctic, scale: 1:6,000,000*, Compiled by: Department of Energy, Ministry of Geology of the USSR, Mines and Resources of Canada.

Karimova, A. A., and S. A. Bornyakov (2021), Examples of segment activation of faults in natural shear zones, in *Proceedings of the XXIX All-Russian Youth Conference "Lithosphere Structure and Geodynamics"*, pp. 126–127, Irkutsk.

Kashubin, S. N., O. V. Petrov, V. A. Poselov, S. P. Shokalsky, E. D. Milshtein, and T. P. Litvinova (2021), Deep Structures of the Circumpolar Arctic, in *Springer Geology*, pp. 29–61, Springer International Publishing, https://doi.org/10.1007/978-3-030-46862-0_2.

Kazanin, O., A. Sidorenko, and C. Drebenstedt (2021), Intensive underground mining technologies: Challenges and prospects for the coal mines in Russia, *Acta Montanistica Slovaca*, *26*(1), 60–69, https://doi.org/10.46544/ams.v26i1.05.

Koronovsky, N. V., G. N. Gogonenkov, M. A. Goncharov, A. I. Timurziev, and N. S. Frolova (2009), Role of shear along horizontal plane in the formation of helicoidal structures, *Geotectonics*, *43*(5), 379–391, https://doi.org/10.1134/s0016852109050033.

Mansurova, S. E. (2010), Numerical modeling of shear strain near to the crack, *Journal of Mining Institute*, *187*, 75–79 (in Russian).

Movchan, I., Z. Shaygallyamova, and A. Yakovleva (2022), Identification of structural control factors of primary gold ore occurrences by method of unmanned aeromagnetic survey by the example of the Neryungrisky district of Yakutia, *Journal of Mining Institute*, *254*, 217–233, https://doi.org/10.31897/pmi.2022.23.

Nikitin, A. A., and A. V. Petrov (2007), Basic procedures of transient fields data processing and interpetation, *Geophysics*, *3*, 63–70 (in Russian).

Petrov, O. V., and M. Poubelier (Eds.) (2019), *Tectonic map of the Arctic*, VSEGEI, St. Petersburg, p. 72.

Prishchepa, O., I. Borovikov, and E. Grokhotov (2021), Oil and gas content of the understudied part in the northwest of the Timan-Pechora oil and gas province according to the results of basin modeling, *Journal of Mining Institute*, *247*, 66–81, https://doi.org/10.31897/pmi.2021.1.8.

Saitgaleev, M. M., G. K. Grigoriev, T. A. Mingaleva, and J. A. Sokolova (2021), Application of a neural network for faults mapping, in *Engineering and Mining Geophysics 2021*, European Association of Geoscientists & Engineers, https://doi.org/10.3997/2214-4609.202152144.

Shtokalenko, M. B. (2018), Improved formula for analytic continuation of the potential field downwards, in *Geology and minerals of the Western Urals*, vol. 18, pp. 218–220, Perm State University.

Sohrabi, A., A. Nadimi, I. V. Talovina, and H. Safaei (2019), Structural model and tectonic evolution of the fault system in the southern part of the Khur area, Central Iran, *Journal of Mining Institute*, *236*(2), 142–152, https://doi.org/10.31897/pmi.2019.2.142.

Tran, T. D., R. G. Kulinich, Q. M. Nguyen, V. S. Nguyen, T. D. Tran, T. T. Nguyen, B. D. Nguyen, T. L. Tran, K. D. Nguyen, X. T. Dang, D. C. Dao, and T. S. Nguyen (2021), Study on reaction possibility of the faults system in the western part of the South China Sea as a source of geological hazards, *Tikhookeanskaya Geologiya*, *40*(6), 68–84, https://doi.org/10.30911/0207-4028-2021-40-6-68-84 (in Russian).

Wherry, R. J. (1984), Measures of Relationship between Two Variables, in *Contributions to Correlational Analysis*, pp. 15–33, Elsevier, https://doi.org/10.1016/b978-0-12-746050-5.50005-1.

Yakovleva, A. A., I. B. Movchan, and Z. I. Shaygallyamova (2022), Dynamic response of multi-scale geophysical systems: waves and practical applications, *Philosophical Transactions of the Royal Society A: Mathematical, Physical and Engineering Sciences*, *380*(2237), https://doi.org/10.1098/rsta.2021.0403.